Integrated Risk Assessment for Monumental Structures under Climate Change and Seismic Hazards

Dimitrios Egglezos[1]

[1]PhD Civil Engineer, GEO.PER SA & Hellenic Open University, Greece, email: englezos.dimitrios@ac.eap.gr

ABSTRACT

Historic monumental structures face increasing vulnerability from climate change and seismic hazards, requiring integrated assessment methods to guide conservation efforts. This paper presents a modular framework that combines climatic degradation modelling with probabilistic seismic hazard analysis (PSHA) to evaluate the evolving condition of monumental masonry. The effective masonry elastic modulus is adopted as the principal screening-level state variable because it is highly sensitive to cracking and loss of composite action and can be transferred directly to equivalent-linear structural assessment; alternative indicators, such as shear modulus or shear-wave velocity, may also be used when suitable monitoring data are available. Material deterioration is reconstructed from current mechanical properties using GSI-based back-analysis, while burial or protection periods are treated as intervals of frozen decay. Climate-driven ageing is then updated through persistence-based indicators derived from historical and projected daily climate series, and seismic effects are represented through past events, future exceedance probabilities, and possible restoration-induced recoveries. For seismic hazard, the framework uses code-consistent zonal hazard and EC8 soil-category information as a first-order site-specific representation, while allowing future refinement through dedicated local site-response studies. The Roman Balneum in Rafina, Greece, is used as a demonstration case. Under the illustrative high-emission climate projection adopted here, climatic forcing accelerates deterioration and yields a moderate-to-high Heritage Risk Index (HRI) by 2100. The method is intended as a decision-support tool under limited data and should therefore be interpreted together with parameter ranges, climate-scenario spread, and sensitivity analyses rather than as a single deterministic forecast.
Keywords: Heritage masonry; elastic modulus; climatic ageing; persistence indicators; salt crystallization; PSHA; Eurocode 8; decision support.

INTRODUCTION

Heritage masonry structures are subjected to long-term deterioration mechanisms induced by environmental actions such as wetting–drying cycles, salt crystallisation, freeze–thaw effects, and thermal fatigue, as well as to seismic actions of varying intensity. These processes are interdependent: progressive climatic degradation reduces material stiffness and strength, thereby increasing seismic vulnerability, while earthquake-induced cracking enhances moisture ingress and accelerates subsequent climate-driven deterioration.

This work proposes an integrated, modular methodology that (a) quantifies the current structural deficit relative to an reconstructed reference state, (b) estimates the climatic contribution to degradation using daily persistence indicators and material/regime sensitivities, (c) accounts for past earthquakes and restoration actions as discrete jumps in stiffness, and (d) represents future seismicity with a PSHA-based probability of exceedance over a decision window. The overall output is a unified Heritage Risk Index (HRI) that supports rational decision making regarding inspection priorities, intervention timing, and the dominant threat to be addressed.

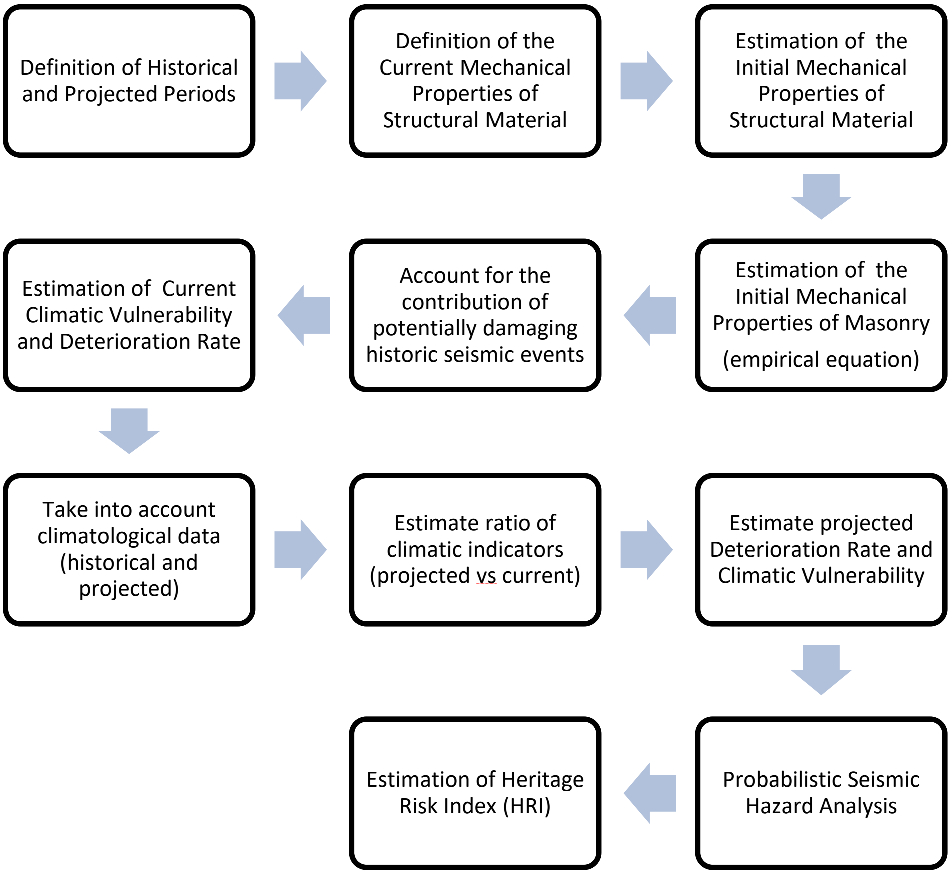

Figure 1. *Workflow of the proposed methodology*

STRUCTURAL STATE VARIABLE AND RECONSTRUCTION OF THE REFERENCE CONDITION

Choice of elastic modulus as the unique degradation variable

The proposed framework adopts the effective elastic modulus of *masonry* as the unique scalar variable representing structural degradation. This choice is motivated by (i) its direct sensitivity to cracking, joint opening, mortar loss, and loss of composite action, (ii) its usability in linear and equivalent-linear analyses, and (iii) its practical link to strength parameters through empirical correlations used in masonry assessment workflows. The choice does not imply that elastic modulus is the only admissible descriptor: shear modulus or shear-wave velocity may also be informative, especially when dynamic testing or continuous monitoring is available. However, neither quantity is inherently superior for the present screening-level objective. In simplified continuum treatment, shear modulus is closely related to elastic modulus through the assumed Poisson coupling, while shear-wave velocity is primarily a measurable diagnostic proxy of stiffness rather than a direct structural-capacity variable. In heterogeneous historic masonry, both quantities are also strongly affected by anisotropy, cracking pattern, confinement, moisture state, and strain level. Accordingly, the elastic modulus is retained here as the most practical common currency linking material degradation, equivalent-linear structural assessment, and intervention planning.

Reconstruction of E_M from current strengths

To avoid over-simplifying the distinct degradation of stones/bricks and mortar, the reconstruction of the initial reference modulus uses two material parameters. Current compressive strengths of the masonry components $f_{cur,cb}$ for units and $f_{cur,cm}$ for mortar) are estimated from tests, classification, or reliable analogies. They are combined into a masonry compressive strength $f_{cur,cM}$ using empirical equations (CEN, 2012; OASP, 2022; Bröcker, 1961; Hendry, 1981; Tassios, 1983; Tassios, 1986).

The current masonry modulus is then obtained as (CEN, 2012; Penelis, 2020):

$$E_{cur,M} = \lambda \cdot f_{cur,cM}$$

The coefficient λ is selected from the literature or local calibration for the masonry typology and units. For the reconstruction of the initial condition, intact values for the components are estimated by setting GSI_b = GSI_m = 100 with appropriate material constants ($m_{i,b}$, $m_{i,m}$), yielding $f_{0,cb}$ and $f_{0,cm}$, and thus $f_{0,cM}$, and $E_{0,cM}$. After this reconstruction step, the subsequent degradation and risk calculations use only the masonry modulus E_M, as a single structural variable.

Zonation and application to structural sub-areas

The same procedure may be applied globally (single representative E_M for the structure) or locally (zoned E_M values for walls, piers, vaults, or distinct material assemblages). Zonation is recommended when distinct exposure conditions and construction typologies coexist, while the global version remains useful for screening-level decision support.

CLIMATIC AGEING MODEL

Effective exposure time and buried periods

Heritage structures may experience long periods of burial/backfill or protection, during which the dominant climatic damage mechanisms are largely suppressed. This is represented through an exposure factor $\zeta(t) \epsilon [0,1]$ and an effective exposure time:

$$t_{eff}(t) = \int_{t_0}^{t} \zeta(t)\, dt$$

For piecewise-constant exposure, t_{eff} reduces to a sum of $\zeta_k\ \Delta t_k$. A buried period is modelled with $\zeta = 0$, resulting in frozen decay during that interval, while $\zeta = 1$ represents a fully exposed site. Intermediate values can represent partial sheltering, maintenance or protective roofing.

Power-law climatic degradation in effective time

A single climatic degradation law is adopted for implementability and calibration with limited data. The stiffness reduction is expressed as a power-law in effective exposure time:

$$E_M(t) = E_{0,M} / \left[1 + \alpha \cdot t_{eff}(t)\right]^m, \ \ \textit{with}\ 1 - \alpha \cdot t_{eff}^m > 0$$

The exponent governs the curvature of degradation versus exposure, while the rate parameter sets the time scale of decay. When only one calibration point is available, the present conference-paper implementation fixes the exponent to 1.0 and calibrates only the rate parameter to match the current condition. This is a parsimonious choice that avoids over-parameterization, preserves identifiability, and corresponds to a constant average loss rate in effective time. Where richer chronological data are available, the exponent should be calibrated explicitly and explored in sensitivity analyses.

Handling abrupt changes (earthquakes and interventions)

Past earthquakes and restoration interventions cause abrupt changes in stiffness. Let a jump occur at time t_j, producing a transition from $E^-(t_J)$ to $E^+(t_J)$. Climatic ageing continues after the jump with the same parameters (a, m), but with a reset initial condition at the jump and with continued effective-time accounting:

$$E_M(t) = E^+(t_J) / \left[1 + \alpha \cdot \left(t_{eff}(t) - t_{eff}(t_j)\right)\right]^m, \quad \textit{for} \qquad t > t_j$$

This separation enables a transparent decomposition into continuous climate-driven ageing and discrete event/intervention effects.

CLIMATIC FORCING

Data and processing window

Climatic forcing is computed from daily series of minimum and maximum temperature (T_N, T_X), precipitation (RR), and relative humidity (RH), for both a historical baseline window and a projected window derived from climate scenario ensembles (e.g., CMIP6 SSPs and IPCC RCP pathways) (Eyring et al., 2016; O'Neill et al., 2016; Riahi et al., 2011; IPCC, 2021). When available, reanalysis datasets such as ERA5 provide dynamically consistent historical daily series (Hersbach et al., 2020), while future projections are typically obtained from bias-corrected and downscaled regional climate products (Teutschbein & Seibert, 2012).

Spell definition and the indicator value used

A spell is defined as a maximal sequence of consecutive days satisfying a condition $X(d) = true$. To be mechanistically meaningful, a minimum spell length q is enforced. Two summaries are possible: spell-count (number of spells per year) and spell-days (number of days that belong to qualifying spells per year).

In the present methodology, the indicator values used in calculations are defined explicitly as follows see also Table 4):

- For Hot Spell Days (HSD3), Wet Spell Days (WSD2) and Freeze Thaw Wet Spell Days (FTWSD2) the indicator value is spell-days per year: the number of days that belong to spells of length at least q.
- For Wet to Dry Transition events (WDTr3) the indicator value is event count per year: each qualifying wet spell may contribute at most one wet-to-hot/dry transition event.

Persistence indicators and mechanistic regimes (C1-C4)

Four persistence indicators are adopted to represent dominant climatic damage mechanisms, grouped into four regimes:

- C1 Hot-Dry: thermal cycling and desiccation shrinkage (notably relevant for timber and earthen materials). Indicator HSD3 counts the number of days per year belonging to spells of at least 3 consecutive days with $T_X \geq T_H$ (default $T_H = 35°C$).
- C2 Coastal/salt: salt solution activation and crystallisation driven by humidity conditions and wetting-drying transitions. Indicator WDTr3 counts wet-to-hot/dry transition events per year, defined as a wet spell ($RR \geq P_0$ for at least 2 consecutive days) followed by at least one hot/dry day ($T_X \geq T_H$ and $RR < P_0$) within a window of 3 days.
- C3 Temperate-Wet: sustained wetting leading to mortar washout/softening, biological colonisation, and moisture-driven microcracking. Indicator WSD2 counts days per year belonging to spells of at least 2 consecutive wet days with $RR \geq P_0$ (default $P_0 = 1\ mm/day$) consistent with the ETCCDI wet-day definition (Zhang et al., 2011).
- C4 Cold-Wet: freeze-thaw under moisture availability and repeated phase change. Indicator FTWSD2 counts days per year belonging to spells of at least 2 consecutive wet-filtered freeze-thaw days, defined by $T_N \leq 0°C, T_X \geq 0°C$ and an antecedent rainfall index $ARI_n \geq ARI_0$ (default $ARI_n = 5\ days$ and $ARI_0 = 10\ mm$).

Salt characterization parameter

The presence and type of soluble salts are incorporated through a salt characterization factor $\kappa_{salt} \in [0,1]$, selected from sampling and visual diagnosis (0: negligible salts; 0.5: moderate/localised efflorescence; 1: widespread active salt decay). A humidity activation proxy may be defined as the annual count of days with $RH \geq RH_{thr}$; for $NaCl$ a representative deliquescence threshold is approximately 75% RH at room temperature (Chen et al., 2001).

Sparse-event handling and regime change factors r_i

When annual event counts are small (e.g., fewer than about 10 spells), percentile-based normalisation becomes statistically weak. In such cases, regime change factors are defined using ratios of multi-year means with small pseudo-counts ε to avoid division instability:

$$r_i = (\bar{I}_i^{proj} + \varepsilon_i)/(\bar{I}_i^{hist} + \varepsilon_i)$$

The regime factors r_{C1}, r_{C3} and r_{C4} are obtained directly from HSD3, WSD2 and FTWSD2. For the salt regime C2, a combined proxy may be formed as $r_{C2} = \sqrt{r_{WDTr} \cdot r_{RH75}}$, multiplied by κ_{salt} when a site-specific salt diagnosis is available.

Climate acceleration factor F_{clim}

Material sensitivity to regimes is encoded by a consolidated D^* vector (D^*_{C1} … D^*_{C4}) whose components sum to 1 (see Table of Appendix A). The climate acceleration factor is then:

$$\mathrm{F_{clim}} = \sum_{\mathrm{i}} D^*_{C_i} \cdot r_{C_i}, \quad \text{with } \sum_{\mathrm{i}} D^*_{C_i} = 1$$

If the projected climate equals the baseline (all $r_{C_i} = 1$), then $\mathrm{F_{clim}} = 1$ exactly. For projections, $\mathrm{F_{clim}}$ may exceed 1, representing accelerated climatic forcing relative to the historical baseline.

PAST SEISMIC EVENTS AND INTERVENTION EFFECTS

Event-level stiffness-loss function

Past earthquakes are represented through cumulative stiffness-loss increments. For an event k with PGA_k and magnitude M_k, the event severity is:

$$f(a_k, M_k) = \left(\frac{a_k - a_{min}}{a_{max} - a_{min}}\right)^p \left(\frac{M_k}{M_{ref}}\right)$$

where a_{min} is a lower threshold below which damage contribution is neglected, a_{max} is a reference catastrophic intensity, M_{ref} is a reference magnitude, and p captures the nonlinear increase of damage with intensity. A practical modelling choice is is $p = 2$, reflecting the strongly nonlinear response of masonry once cracking initiates.

Cumulative past loss and repair recovery

The event-level stiffness-loss increment is $\Delta P_{s,k} = \kappa_s f(a_k, M_k)$, where κ_s is a calibration factor representing the maximum plausible fractional stiffness loss for the masonry typology. Post-event interventions are represented by a recovery fraction $\rho_{r,k} \in [0,1]$ applied to each event contribution:

$$\Delta P_s^{past} = \sum_k (1 - \rho_{r,k}) \Delta P_{s,k}$$

This formulation remains simple while preserving the rational feature that a sequence of moderate events can exceed the cumulative impact of a single smaller event.

FUTURE SEISMIC RISK: PSHA-BASED EXCEEDANCE PROBABILITY

For future risk, individual earthquake occurrences are not predicted; instead, probabilistic seismic hazard analysis (PSHA) provides the annual rate of exceedance $\lambda(a_g)$ for a chosen PGA threshold a_g. Under a Poisson occurrence model, the probability of at least one exceedance in a future window T_{proj} is (Cornell, 1968):

$$S(a_g, T_{proj}) = 1 - e^{-\lambda(a_g) T_{proj}}$$

Two thresholds are considered: (i) a damage-onset level $a_{g,onset}$ associated with the onset of substantial cracking and stiffness degradation in masonry, and (ii) a catastrophic level $a_{g,cat}$ representing rare but highly damaging shaking.

EC8-based scaling from $a_{g,475}$ to return period $T_R(a_g)$

When only the code-map reference value is known (475-year return period; 10% probability of exceedance in 50 years), an EC8-based approximation is used to relate the importance factor to return period through the standard exponent adopted in code-oriented practice. This approximation is retained here because the seismic module is intended for screening and comparative prioritization rather than for a detailed performance-based design calculation.

$$\gamma_I = \left(T_{R,ref}/T_R\right)^{1/k} \qquad \text{and} \qquad a_g = \gamma_I \cdot a_{g,475}$$

Rearranging yields an approximate return period for a threshold a_g:

The resulting $S(a_g, T_{proj})$ is a scalar in [0,1] with a transparent interpretation as the probability of at least one exceedance in the decision window.

HERITAGE RISK INDEX (HRI): CURRENT AND PROJECTED

Current vulnerability

The current vulnerability is defined from the reconstructed reference modulus and the current modulus as:

$$C_{cur} = 1 - E_{cur,M}/E_{0,M}$$

Projected index with explicit climate-seismic interaction

For a projection horizon T_{proj}, climatic ageing yields a projected modulus $E_{proj,M}$ and a corresponding vulnerability $C_{proj} = 1 - E_{proj,M}/E_{0,M}$. Future seismicity is represented by $S(a_g, T_{proj})$. A unified index including explicit interaction is defined as:

$$HRI_{proj} = w_C \cdot C_{proj} + w_S \cdot S + w_{CS} \cdot \left(C_{proj} \cdot S\right), \quad \text{with} \quad w_C + w_S + w_{CS} = 1$$

The climatic, seismic, and interaction weights are selected from the heuristic values contained in Appendix B and are indexed by climatic regime (C1-C4) and seismicity class. These are not universal physical constants; they are screening-level decision weights constructed to satisfy three monotonic rules: (i) the seismic contribution increases with seismicity class, (ii) the climatic contribution dominates in low-seismic environments and decreases as expected seismic demand grows, and (iii) the interaction term remains non-zero, and is slightly higher for coastal/salt and cold-wet regimes, to reflect stronger coupling. In practical use, the HRI should be reported together with a sensitivity check on plausible perturbations of these weights.

Use of E_{proj} for equivalent-linear analyses

The projected modulus $E_{proj,M}$ is intended for equivalent-linear structural analyses representing the degraded stiffness state in the selected future period. For example, response-spectrum or linear static analyses may be performed using $E_{proj,M}$ to estimate demand measures and compare to performance thresholds.

UNCERTAINTY, CONFIDENCE, AND RECOMMENDED REPORTING

The method is designed to remain implementable under limited data; however, uncertainties arise from reconstruction of the reference condition, calibration of the degradation law, selection of seismic-loss and recovery parameters, and climatic forcing derived from finite records and scenario assumptions. In the Rafina demonstration, climate change is represented by a single regional climate-model chain under RCP 8.5; this should be interpreted as an illustrative upper-bound scenario rather than as a probabilistic forecast. A fuller implementation should propagate uncertainty through multiple scenarios and, where available, multiple climate models, together with sensitivity analyses on the degradation exponent, decay rate, seismic-loss parameters, and HRI weights. Practitioners are therefore encouraged to report plausible parameter ranges, scenario spread, and confidence levels for any key material or site assumptions.

EXEMPLARY CASE STUDY: ROMAN BALNEUM IN RAFINA

Site characteristics and structural context

The Balneum consists of mixed brick–stone masonry walls exhibiting visible cracking and mortar deterioration. A detailed description of the site geometry, construction phases and hazard exposure conditions is provided in Tzannidakis et al. (2025). Excavation and exposure of the monument after a large burial period (estimated 5th century AD – 1974 AD) occurred primarily after the 1970s (Katakis, 2020). Consequently climatic ageing is treated as active only during the exposed periods ($\zeta = 1$), while burial phase is represented as frozen decay interval (exposure factor $\zeta = 0$).

A potentially damaging earthquake ($M = 5.9$) occurred in 1999 (ParnItha), therefore there are two effective exposure periods: 1974-1999 ($\Delta t_1 = 26\, years$) and 1999-2025 ($\Delta t_2 = 27\, years$). The historical period for the climatic data is the 25 years period of 1981-2005, while the projected period is the 75 years period 2026-2100. The above are summarized in Table 1.

Table 1. *Exposure and burial periods of the Roman Balneum in Rafina.*

Purpose	Period	Δt (Years)	Role in calculations
Construction and exposure	1st/2nd to 5th century AD		Estimation of the aging factor a (continuous material degradation) ($\zeta = 1$)
Burial (estimated)	5th to 1974		Estimation of the aging factor a (time period with slow / non-existent material degradation) ($\zeta = 0$)
Historical Period	1981–2005	25	Computation of historical climatic indicators and baseline degradation calibration
Structural exposure interval 1	1974–1999	26	Climatic ageing before the 1999 earthquake
Parnitha Seismic Event	1999	-	Jump in strength decay due to Seismic event
Structural exposure interval 2	1999–2025	27	Climatic ageing after earthquake and repair
Projection horizon	2026–2100	75	Projection of climatic data and stiffness, and seismic exceedance probability

According to the New Seismic Hazard Map of Greece (OASP, 2003), the Roman Balneum is located in a zone of moderate seismicity, while the site is classified as soil class B. Therefore, the design peak ground acceleration for the regulatory event with 475-year return period is 0.24 g (CEN, 2004), corresponding to the high end of the moderate seismicity class S3 used in Appendix B. For the present conference-paper application, seismic hazard is treated at screening level through the national hazard map and the EC8 soil class assigned to the site. This provides a first-order site-specific representation consistent with code-based practice, but it does not replace a dedicated local site-response or microzonation study. Where soft deposits, basin effects, topographic amplification, or monument-specific intervention design are critical, the same framework can accommodate refined site-specific spectra or amplification factors.

The mechanical properties of the structural materials should ideally be derived from in-situ and/or laboratory testing. In the absence of such investigation, as in the present demonstration of the Roman Balneum, established bibliographic sources can be used for a screening-level assessment

(Penelis, 2020). For the stone units, a limestone compressive strength of 20 MPa was selected (Robertson, 1982); for brick, the average compressive strength of Roman bricks was taken as 9.3 MPa (Penelis, 2020); and for mortar, the average compressive strength of the mortar from the Roman phase of the Rotunda in Thessaloniki was taken as 2.3 MPa (Penelis, 2020).

To backtrack and estimate the initial mechanical properties of the aforementioned materials (stone, brick, mortar) the Geological Strength Index and the Hoek-Brown failure criterion were used (Hoek, 1980; Hoek, 2002; Marinos, 2000; Marinos, 2001). Stone units were treated as limestone rock-mass with current $GSI = 85$, while bricks were treated as material with $m_i = 17$, and current $GSI = 80$. Similarly, mortar was treated as material with $m_i = 17$, and current $GSI = 85$. The estimation of the initial mechanical properties of the structural units is present in Table 2.

Table 2. *Structural materials, mechanical properties and current climatic vulnerability (C)*

Structural Material	GSI_{cur}	Compressive Strength (MPa)	
		Current ($f_{cur,c}$)	Initial ($f_{0,c}$)
Limestone	85	20	46.1
Brick	80	9.3	28.3
Mortar	85	2.3	5.3

Using the values of intact mechanical properties of the structural material (Table 2), masonry strength can be estimated from empirical equations (Bröcker, 1961; Hendry, 1981; Tassios, 1983; Tassios, 1986). The average masonry strength that derives from the aforementioned empirical equations are presented in Table 4. Then the modulus of elasticity is estimated with $\lambda = 750$ (CEN, 2005; Penelis, 2020).

Consideration of past earthquake event (Parnetha, 1999)

To account for the damage contribution of past seismic events (Table 3) to the present structural condition, the degradation trajectory includes a discrete stiffness-loss jump associated with the seismic event. There are no evidence of subsequent structural repair or strengthening interventions in the present condition; therefore, the stiffness reduction produced by the event is considered permanent.

Table 3. *Historic Seismicity (Adapted from Papazachos & Papazachou, 2003)*

Year	Epicenter	Dist (Km)	Magnitude	PGA^1 (G)	PGA^2 (G)	PGA^3 (G)	Pga_{av} (G)
74	**Corinth**	**68.0**	**6.3**	**0.028**	**0.036**	**0.038**	**0.034**
521	Corinth	68.0	6.3	0.028	0.036	0.038	0.034
543	Corinth	68.0	6.2	0.025	0.034	0.034	0.031
580	Corinth	68.0	6.3	0.028	0.036	0.038	0.034
1300	Corinth	68.0	6.0	0.021	0.028	0.028	0.026
1321	Theba	68.0	6.5	0.036	0.044	0.049	0.043
1417	Chalkida	45.7	6.4	0.051	0.065	0.065	0.060
1694	Chalkida	60.7	6.2	0.030	0.040	0.040	0.037
1705	Ne Attica	34.9	6.3	0.063	0.082	0.077	0.074
1725	Corinth	88.5	6.0	0.015	0.020	0.021	0.019
1726	Chalkida	63.7	6.0	0.022	0.031	0.030	0.028
1775	Corinth	97.2	6.2	0.016	0.021	0.023	0.020
1785	Chalkida	54.8	6.0	0.027	0.038	0.035	0.033
1805	Athens	34.2	6.0	0.404	0.349	0.376	0.057
1837	Saronic Bay	72.7	6.4	0.029	0.036	0.040	0.035
1853	Theba	67.2	6.5	0.035	0.044	0.048	0.042
1858	Corinth	99.4	6.5	0.021	0.026	0.031	0.026
1874	Athens	57.7	6.0	0.025	0.035	0.033	0.031
1876	Corinth	107.9	6.1	0.013	0.017	0.018	0.016
1894	Martino	74.2	6.6	0.034	0.042	0.048	0.041
1894	Atalanti	89.4	7.0	0.041	0.045	0.061	0.049
1914	Chalkida	66.0	6.0	0.021	0.030	0.029	0.027

1928	Corinth	89.7	6.3	0.020	0.025	0.028	0.024
1930	Saronic Bay	92.4	6.0	0.014	0.019	0.020	0.018
1938	Oropos	35.1	6.0	0.046	0.063	0.055	0.055
1965	Corinthean Bay	190.4	6.4	0.008	0.009	0.013	0.010
1981	**Alkionides**	**87.6**	**6.7**	**0.031**	**0.036**	**0.045**	**0.037**
1999	**Parnitha**	**40.4**	**5.9**	**0.035**	**0.050**	**0.043**	**0.043**

(1) Scarlatoudis (2003), (2) Rinaldis (1998), (3) Modified Mercalli Intensity: Koliopoulos (1998). PGAav: Average value of PGA as estimated from (1), (2) and (3).

Among the seismic events occurring during the exposed periods, the 1999 Parnitha earthquake exhibited the highest estimated average peak ground acceleration (PGA). The corresponding ground motion at the monument, estimated from the adopted attenuation relationships, is approximately 0.043 g. This value remains below the adopted minimum damage-activation threshold of 0.05 g. Consequently, no discrete seismic-induced degradation (stiffness jump) is introduced in the mechanical evolution model, and stiffness continuity across the event time is assumed. This treatment is intentionally conservative and screening-oriented; if local amplification analyses or instrumental records become available, the event-level PGA values can be updated directly without changing the framework.

Climatic indicators from uploaded daily series

The climatic vulnerability (C) which is presented in Table 4 is estimated by modulus of elasticity of the initial and current condition. The Roman Balneum was built somewhere in early Roman Period (1st–2nd century AD) on earlier remains (5th–4th BC) while evidence place the latest usage of the site somewhere in the early 3rd century AD (Katakis, 2020). A rough estimation on the time of the exposure of the site to natural phenomena (pre-burial period) is about 400 years. Taking into account the above the estimated deterioration rate α is presented in Table 4.

Table 4. *Structural materials, mechanical properties and current climatic vulnerability (C)*

Masonry Type	**Compressive Strength (MPa)**		**Modulus of Elasticity (GPa)**		**Climatic Vulnerability (C)**	**Deterioration rate ($\alpha; years^{-1}$)**
	Current ($f_{cur,M}$)	**Initial ($f_{0,M}$)**	**Current ($E_{cur,M}$)**	**Initial ($E_{0,M}$)**		
Stone	4.25	8.21	3.2	6.2	0.484	0.00107
Brick	2.61	5.55	2.0	4.2	0.524	0.00116
Mixed	3.43	6.88	2.6	5.2	0.500	0.00110

Daily historical (1981-2005) and projected (2026-2100) climate series were obtained from the DEAR-Clima database (DEAR-Clima, 2023). The projected data used in the Rafina demonstration correspond to one illustrative high-emission chain (RCP 8.5; MPI-CSC-REMO2009 driven by MPI-ESM-LR) and are treated here as a stress-test scenario rather than as an exhaustive representation of climate uncertainty. The data are then processed using the previously defined spell indicators and transition criteria. Table 5 summarises the resulting multi-year mean indicator values, ratios, and units.

Table 5. *Climatic persistence indicators used in the Rafina demonstration (historical vs projected RCP8.5 periods)*

Indicator	**Description**	**Units**	**Historical mean (1981–2005)**	**Projected mean (2026-2100)**	**Ratio r_i $\frac{Projected}{Historical}$**
HSD3	Hot-spell days (≥3 consecutive hot days)	days/year	22.2	56.51	2.54
WDTr3	Wet-to-dry transition events within 3 days	events/year	0.24	0.57	2.41
WSD2	Wet-spell days (≥2 consecutive wet days)	days/year	33.62	24.95	0.74
FTWSD2	Wet freeze–thaw spell days (≥2 consecutive days)	days/year	—	—	1.00 (no change)

RH	Relative Humidity	%	64.17	64.28	1.00

As already mentioned r_{C1}, r_{C3}, and $r_{C4}$are equal to r_{HSD3}, r_{WSD2} and r_{FTWSD2} respectively, while $r_{C2} = \sqrt{r_{WDTr} \cdot r_{RH75}} = \sqrt{2.41 \cdot 1.00} = 1.55$

Projected deterioration rate and vulnerability at the end of the century

Regime change factors are computed using the ratio formulation. The climate acceleration factor is then obtained from the appropriate material-sensitivity vector, and the historical deterioration rate is scaled accordingly over the selected decision window. Because the rate parameter is site- and material-dependent, the projected values reported here should be interpreted as scenario-conditioned estimates rather than universal constants.

As already stated, $\mathrm{F_{clim}} = \sum_{\mathrm{i}} D^*_{C_i} \cdot r_{C_i}$, with $\sum_{\mathrm{i}} D^*_{C_i} = 1$ and $D^*_{C_i}$ for masonry walls is given in the table of Appendix A. For each type of masonry $\mathrm{F_{clim}}$ is presented in Table 6. The deterioration rate, the climatic vulnerability of masonry walls and the estimated mechanical properties in the projected period are presented in Table 6.

Table 6. *Deterioration rate and vulnerability of masonry walls by the end of the projected period (2100)*

Masonry Type	F_{clim}	Projected Deterioration rate (α_{2100}; years^{-1})	Projected Climatic Vulnerability (C_{2100})	Projected Compressive Strength ($f_{2100,M}$; MPa)	Projected Modulus of Elasticity ($E_{2100,M}$; GPa)
Stone	1.26	0.00135	0.585	3.41	2.57
Brick	1.28	0.00148	0.635	2.02	1.53
Mixed	1.27	0.00141	0.606	2.71	2.05

From the findings of Table 6 it is clear that under RCP8.5 in the projected period (2026–2100) the climate-driven deterioration rate is accelerated by about +27% relative to the historical period.

Seismic Hazard by the end of the projected period

Using the EC8-consistent reference PGA and a 75-year decision window (2026-2100), the probability of exceedance of the regulatory seismic threshold is approximately 0.146. This probability is used here as a screening-level seismic-risk metric and can be replaced directly by a site-specific PSHA result where such information is available.

Estimation of the final Heritage Risk Index (HRI)

Using the default Appendix B weights for the relevant climatic regime and seismicity class, and taking the mixed masonry as a representative average, the Heritage Risk Index of the Rafina Balneum is estimated as 0.36. This value should be interpreted as a screening-level prioritization index rather than as an exact deterministic forecast, and its robustness should be checked through reasonable perturbations of the adopted weights and deterioration parameters.
Since HRI_{2100} is a normalized index in the range 0–1, a value of $0.355 \approx 0.36$ represents a moderate-to-high integrated risk level for the 2100 horizon. A HRI classification table is presented in Appendix C.

CONCLUSIONS AND DECISION-SUPPORT PERSPECTIVE

This study presented a modular methodology for the integrated assessment of heritage structural risk under combined climatic deterioration and seismic hazard, using the effective masonry modulus as a single structural state variable. The approach enables reconstruction of the initial mechanical condition from present measurements, calibration of historical degradation through effective exposure time accounting (including burial periods with frozen decay), and projection of future deterioration by incorporating climate-change-induced acceleration factors derived from persistence-based climatic indicators.

Application of the framework to the Roman Balneum of Rafina demonstrated the practicality of the method under realistic data constraints, although it should be regarded as a methodological demonstration rather than a full validation exercise. The analysis indicated that, although the seismic hazard at the site corresponds to a moderate seismicity class, the projected increase in climatic forcing - primarily associated with increased thermal persistence and wet-to-dry transition cycles - produces a significant acceleration of the long-term deterioration rate. As a result, the projected structural vulnerability increases substantially by the end of the twenty-first century, leading to a Heritage Risk Index of about 0.36, which falls in the moderate-to-high range. The decomposition of the HRI components shows that climate-driven ageing is the dominant contributor to the projected risk, while seismicity acts mainly as a conditional triggering hazard whose importance increases as structural vulnerability accumulates over time. Within this integrated-risk setting, the use of elastic modulus as the primary state variable remains operationally advantageous because it provides a direct bridge between observed degradation and structural analysis, whereas shear-wave-based quantities are better viewed as possible monitoring inputs or calibration aids.

The methodology offers several practical advantages for conservation decision support. First, it allows consistent comparison of present and future risk levels under different climate scenarios using a unified index. Second, it identifies the dominant deterioration mechanisms governing risk evolution, enabling targeted preventive interventions such as moisture control, desalination, or protective sheltering where climatic processes dominate, or structural strengthening where seismic vulnerability is critical. Third, the framework is scalable, allowing both screening-level assessments using limited data and more detailed zoned analyses when site-specific monitoring or laboratory characterization is available.

Future work should focus on (i) calibrating deterioration parameters through laboratory-based material-ageing experiments and long-term monitoring datasets, (ii) comparing the HRI predictions with observed damage evolution and alternative structural indicators, (iii) propagating uncertainty through multi-scenario and multi-model climate ensembles, (iv) refining the seismic module through local site-response or microzonation studies where warranted, and (v) integrating economic optimization modules to support cost-benefit prioritization of conservation strategies. Together, these developments will enhance the reliability of predictive heritage risk modelling and support proactive preservation planning for historic masonry structures exposed to increasingly coupled environmental and seismic threats.

ACKNOWLEDGEMENTS

I would like to thank Mr Manolis Tzannidakis, Civil Engineer (MSc), for his assistance with the preparation of the illustrative material and the formatting of the manuscript.

REFERENCES

Bröcker O., 1961, Steinfestigkeit und Wandfestigkait Betonstein Zeitung 27, Heft 3.

CEN (2004). EN 1998-1: Eurocode 8 - Design of structures for earthquake resistance - Part 1: General rules, seismic actions and rules for buildings and Greek National Annex. European Committee for Standardization, Brussels.

CEN (2005). EN 1996-1-1: Eurocode 6, Design of Masonry Structures-Part 1-1: General Rules for Reinforced and Unreinforced Masonry Structures, European Committee for Standardization, Brussels.

CEN (2012). Eurocode 6: Design of masonry structures – Part 1-1: General rules for reinforced and unreinforced masonry structures (EN 1996-1-1:2005+A1:2012), European Committee for Standardization, Brussels.

Chen, Y. Y., Kreidenweis, S. M., McInnes, L. M., Rogers, D. C., & DeMott, P. J. (2001). The effect of surfactants on the deliquescence of sodium chloride aerosol at approximately 75% relative humidity. Journal of Geophysical Research: Atmospheres, 106(D7), 6833–6842. DOI: https://doi.org/10.1029/2000JD900545.

Cornell, C.A. (1968). Engineering Seismic Risk Analysis. Bulletin of the Seismological Society of America, 58(5), 1583-1606.

DEAR-Clima (2023). Data Extraction Application for Regional Climate (DEAR-Clima). Aristotle University of Thessaloniki / GEO-CRADLE Project. Available at: http://meteo3.geo.auth.gr:3838/ and http://datahub.geocradle.eu/dataset/dear-clima/resource/f9b299f0-2ae1-49f4-8a0e-88bdd3aa6899 (Last Accessed: 2026 Jan. 12).

Eyring, V., et al. (2016). Overview of the Coupled Model Intercomparison Project Phase 6 (CMIP6). Geoscientific Model Development, 9, 1937–1958.

Giorgetta, M.A., et al. (2013). Climate and carbon cycle changes from 1850 to 2100 in MPI-ESM simulations for the Coupled Model Intercomparison Project Phase 5. Journal of Advances in Modeling Earth Systems, 5, 572–597.

Hendry, A. W. (1981). Structural Masonry. London: Macmillan Press.

Hersbach, H., et al. (2020). The ERA5 global reanalysis. Quarterly Journal of the Royal Meteorological Society, 146(730), 1999–2049.

Hoek, E., & Brown, E. T. (1980). Underground excavations in rock. Institution of Mining and Metallurgy, London.

Hoek, E., Carranza-Torres, C., & Corkum, B. (2002).Hoek–Brown failure criterion—2002 edition. Proceedings of the North American Rock Mechanics Symposium, Toronto.

IPCC (2014). Climate Change 2014: Synthesis Report.

IPCC (2021). Climate Change 2021: The Physical Science Basis. Contribution of Working Group I to the Sixth Assessment Report of the IPCC (Summary for Policymakers).

Jacob, D. (2001). A note to the simulation of the annual and inter-annual variability of the water budget over the Baltic Sea drainage basin. Meteorology and Atmospheric Physics, 77, 61–73.

Jacob, D., et al. (2012). EURO-CORDEX: new high-resolution climate change projections for European impact research. Regional Environmental Change, 14, 563–578.

Katakis SE, Vasiadi S (2020) The Roman Baths of Rafina: Research at the archaeological site. Rafina – Pikermi the centuries – long history of an Attic land. pp 141-173.

Koliopoulos, P.K., Margaris, B.N. & Klimis, N.S. (1998). Duration and energy characteristics of Greek strong motion records. Journal of Earthquake Engineering, 2(3), 391–417.

Marinos, P., & Hoek, E. (2000). GSI: A geologically friendly tool for rock mass strength estimation. In Proceedings of GeoEng 2000: International Conference on Geotechnical & Geological Engineering (pp. 1422–1446). Melbourne, Victoria, Australia: Technomic Publishing Company.

Marinos, P., Hoek, E., 2001. Estimating the geotechnical properties of heterogeneous rock masses such as flysch. Bull. Eng. Geol. Environ. 60, 85–92.

OASP (2003). New Seismic Hazard Map of Greece. Organization for Anti-Seismic Planning and Protection (OASP), Athens, Greece.

O'Neill, B.C., et al. (2016). The Scenario Model Intercomparison Project (ScenarioMIP) for CMIP6. Geoscientific Model Development, 9, 3461–3482.

Papazachos, B.C. & Papazachou, C.B., 2003. The earthquakes of Greece. Ziti Publications, Thessaloniki, Greece, 286 pp.

Penelis, G.G., Penelis, G.G., (2020), Structural Restoration of Masonry Monuments: Arches, Domes and Walls, 1st edition, CRC Press, eBook ISBN 9780429024030, 370 p.

Robertson, E. C. (1982). Physical Properties of Building Stone. In Conservation of Historic Stone Buildings and Monuments (pp. 62–86). Washington, DC: The National Academies Press.DOI: https://doi.org/10.17226/514.

Riahi, K., et al. (2011). RCP 8.5 — A scenario of comparatively high greenhouse gas emissions. Climatic Change, 109, 33–57.

Rinaldis, D., Berardi, R., Theodulidis, N.P. & Margaris, B.N. (1998). Empirical predictive models based on a joint Italian and Greek strong motion database: I. Peak ground acceleration and velocity. In Proceedings of the 11th European Conference on Earthquake Engineering (CD-ROM), Paris.

Skarlatoudis, A.A., Papazachos, C.B., Scordilis, E.M. & Karakostas, V. (2003). Empirical peak ground-motion predictive relations for shallow earthquakes in Greece. Bulletin of the Seismological Society of America, 93(6), 2591–2606.

Tassios, T.P., Vintzileou, E.N. & Trochanis, A., 1983. Draft Regulation for the Design of Masonry Buildings. Ministry of Public Works (ΥΔΕ), Atheαs, Greece.

Tassios TP, Chronopoulos MP (1986), Aseismic dimensioning of interventions (repairs/strengthening) on low-strength masonry building, Middle East and Mediterranean Regional Conference on Earthen and lowstrength masonry buildings in seismic areas, Ankara.

Teutschbein, C., & Seibert, J. (2012). Bias correction of regional climate model simulations for hydrological climate-change impact studies: Review and evaluation of different methods. Journal of Hydrology, 456–457, 12–29. DOI: https://doi.org/10.1016/j.jhydrol.2012.05.052.

Tzannidakis, E., Egglezos, D., & Moullou, D. (2025). Evaluation of natural hazard risk on monumental structures: The case of the Rafina's Roman Bath Complex in Attica, Greece. In G. Pavlidis & S. Sylaiou (Eds.), Transforming heritage research in a transforming world: 5th CAA-GR Conference 2024 (pp. 91–102). Springer.DOI 10.1007/978-3-032-06389-2_9.

Zhang, X., Alexander, L., Hegerl, G.C., Jones, P., Tank, A.K., Peterson, T.C., Trewin, B., & Zwiers, F.W. (2011). Indices for monitoring changes in extremes based on daily temperature and precipitation data. Wiley Interdisciplinary Reviews: Climate Change, 2(6), 851–870.

Appendix A. Consolidated matrix (materials x climatic regimes C1-C4)

Table A1 provides default regime weights for the climate-acceleration factor. Each row sums to 1.0 and may be adjusted when material properties, salt exposure, monitoring evidence, or observed damage justify deviations.

Table A1. *Default consolidated $\boldsymbol{D}^*$ matrix (from the implementation workbook).*

Material	C1 Hot-Dry	C2 Coastal/salt	C3 Temperate-Wet	C4 Cold-Wet
Porous stone	0.15	0.25	0.35	0.25
Sandstone	0.10	0.30	0.35	0.25
Porous limestone	0.10	0.35	0.30	0.25
Dense limestone	0.15	0.30	0.25	0.30
Marble	0.30	0.30	0.20	0.20
Granite	0.20	0.15	0.25	0.40
Timber	0.25	0.15	0.35	0.25
Bricks (fired)	0.10	0.30	0.30	0.30
Mud bricks (adobe)	0.10	0.25	0.45	0.20
Lime mortar	0.15	0.30	0.30	0.25
Mud mortar	0.10	0.25	0.45	0.20
Pozzolanic mortar	0.15	0.25	0.25	0.35
Brick Masonry	0.115	0.300	0.300	0.285
Stone Masonry	0.115	0.335	0.300	0.250
Mixed	0.115	0.3175	0.300	0.2675

Appendix B. Recommended weights table (climatic regime x seismicity class)

Appendix B gives screening-level default weight triplets for climatic, seismic, and interaction terms. The seismic weight increases from S1 to S5, the climatic weight decreases accordingly, and the interaction term is slightly higher for coastal/salt and cold-wet regimes.

Table B1. *Weight lookup table: each cell lists $\boldsymbol{w_C}$/ $\boldsymbol{w_S}$ / $\boldsymbol{w_{CS}}$ (sum = 1).*

Climatic regime	S1 <0.05g	S2 0.05–0.10g	S3 0.10–0.20g	S4 0.20–0.30g	S5 >0.30g
C1 Hot–Dry	0.77/0.14/0.10	0.68/0.23/0.10	0.54/0.36/0.10	0.40/0.50/0.10	0.27/0.63/0.10
C2 Coastal/salt	0.68/0.12/0.20	0.60/0.20/0.20	0.48/0.32/0.20	0.36/0.44/0.20	0.24/0.56/0.20
C3 Temperate–Wet	0.75/0.13/0.12	0.66/0.22/0.12	0.53/0.35/0.12	0.40/0.48/0.12	0.26/0.62/0.12
C4 Cold–Wet	0.70/0.12/0.18	0.61/0.21/0.18	0.49/0.33/0.18	0.37/0.45/0.18	0.25/0.57/0.18

Appendix C. HRI Characterisation

Table C1. *HRI characterisation table.*

HRI Range	Risk Level	Interpretation
0.00-0.20	Low	Negligible integrated hazard effect; no immediate intervention required
0.20-0.40	Moderate	Noticeable integrated hazard influence; monitoring recommended
0.40-0.60	High	Significant multi-hazard impact; mitigation planning advised
0.60-0.80	Very High	Critical combined hazard exposure; intervention prioritised
0.80-1.00	Extreme	Severe integrated risk; urgent structural action required